CrossMark

Development and Production of Array Barrier Detectors at SCD

P.C. KLIPSTEIN [iD],[1,3] E. AVNON,[1] Y. BENNY,[1] E. BERKOWICZ,[1]
Y. COHEN,[1] R. DOBROMISLIN,[1] R. FRAENKEL,[1] G. GERSHON,[1]
A. GLOZMAN,[1] E. HOJMAN,[1] E. ILAN,[1] Y. KARNI,[1] O. KLIN,[1]
Y. KODRIANO,[1] L. KRASOVITSKY,[1] L. LANGOF,[1] I. LUKOMSKY,[1]
I. NEVO,[1] M. NITZANI,[1] I. PIVNIK,[1] N. RAPPAPORT,[1] O. ROSENBERG,[1]
I. SHTRICHMAN,[1] L. SHKEDY,[1] N. SNAPI,[1] R. TALMOR,[1] R. TESSLER,[1]
E. WEISS,[1] and A. TUITO[2]

1.—SemiConductor Devices, PO Box 2250, 31021 Haifa, Israel. 2.—Israel MOD, Tel Aviv, Israel.
3.—e-mail: philip_k@scd.co.il

XBn or XBp barrier detectors exhibit diffusion-limited dark currents comparable with mercury cadmium telluride Rule-07 and high quantum efficiencies. In 2011, SemiConductor Devices (SCD) introduced "HOT Pelican D", a 640×512/15-μm pitch InAsSb/AlSbAs XBn mid-wave infrared (MWIR) detector with a 4.2-μm cut-off and an operating temperature of ~150 K. Its low power (~3 W), high pixel operability (>99.5%) and long mean time to failure make HOT Pelican D a highly reliable integrated detector-cooler product with a low size, weight and power. More recently, "HOT Hercules" was launched with a 1280×1024/15-μm format and similar advantages. A 3-megapixel, 10-μm pitch version ("HOT Blackbird") is currently completing development. For long-wave infrared applications, SCD's 640×512/15-μm pitch "Pelican-D LW" XBp type II superlattice (T2SL) detector has a ~9.3-μm cut-off wavelength. The detector contains InAs/GaSb and InAs/AlSb T2SLs, and is fabricated into focal plane array (FPA) detectors using standard production processes including hybridization to a digital silicon read-out integrated circuit (ROIC), glue underfill and substrate thinning. The ROIC has been designed so that the complete detector closely follows the interfaces of SCD's MWIR Pelican-D detector family. The Pelican-D LW FPA has a quantum efficiency of ~50%, and operates at 77 K with a pixel operability of >99% and noise equivalent temperature difference of 13 mK at 30 Hz and F/2.7.

Key words: Infrared detector, barrier detector, XBn, XBp, megapixel, MWIR, LWIR, type II superlattice

INTRODUCTION

SemiConductor Devices (SCD) has been manufacturing InSb-based mid-wave infrared (MWIR) focal plane array (FPA) detectors for more than 20 years. These detectors are based on an ion-implanted p–n junction and the technology has been continuously improved to enable the production of larger format, smaller pitch arrays such as the Blackbird 1920×1536/10-μm FPA which was recently launched on our production line. InSb FPAs are extremely uniform due to the very high quality of the binary semiconductor material and the simplicity and regularity of the pixelation process. For this reason, they are very much in demand for large area surveillance, missile warning and other applications requiring a highly scalable process with very few pixel defects.[1] However, because the dark current in the p–n junction is limited by generation–recombination (G–R) processes that occur through Shockley–Read–Hall (SRH) traps with energies near the middle of the semiconductor bandgap, the operating temperature for implanted InSb devices is limited to

$\sim$80 K. In 2006, SCD introduced its epi-InSb line of detectors which operate at 95 K with the same dark current and overall performance as the implanted InSb detectors. The higher operating temperature was achieved by using a p–n junction grown by molecular beam epitaxy (MBE), in which the number of SRH traps is reduced relative to the number produced in the ion-implantation process. Nevertheless, the dark current is still G–R-limited and, in order to raise the operating temperature further, or to increase the operating wavelength, SCD has established two new lines of detector, each of which is based on a patented barrier device architecture grown by MBE on GaSb substrates.

The first line is a MWIR XBn detector with an InAsSb active layer (AL) and an AlSbAs barrier layer (BL).[2,3] The symbol "X" is used for the contact layer (CL) which can be grown p-type or n-type and is InAsSb or GaSb.[4] "B" represents the barrier layer (BL) and "n" is the n-type AL. The AL material is an alloy of InSb and InAs and G–R currents are suppressed by using a BL which has the same n-type doping as the AL and a valence band which is close in energy to that of the AL.[5] Minority holes excited by the absorption of light in the AL can thus diffuse without obstruction into the BL where they drift to the CL under the influence of the internal barrier electric field. The detector bias is chosen to ensure that the AL is close to a flat band condition with no depletion, so that no G–R currents are produced there. Electrically, the device operates like a wide bandgap detector with a very low G–R current characteristic of the wide band gap BL, while optically the device is similar to a narrow bandgap detector. The device operates at 150 K with a cut-off wavelength of $\sim$4.2 μm and is produced today with a 15-μm pitch in formats from 640 $\times$ 512 for "HOT Pelican D" to 1280 $\times$ 1024 for "HOT Hercules". A "HOT Blackbird" version (1920 $\times$ 1536/10 μm) has also been developed.[6]

The second line of detectors is a LWIR XBp detector in which two different p-doped type II superlattices are used, InAs/GaSb for the AL and InAs/AlSb for the BL. The operating principles are similar to those for the MWIR XBn devices described above. The first product is "Pelican-D LW" which has a cut-off wavelength of 9.3 μm, a pitch of 15 μm and operates at 77 K. It has a format of 640 $\times$ 512 as for the other "Pelican" lines, and the customized digital ROIC has been carefully designed so that the complete detector closely adheres to the same interfaces, enabling fast system integration.

In this paper, a short overview will be presented of the MWIR XBn and LWIR XBp detector lines. Some of the key design features will be discussed, including layer doping, band alignment and response optimization.

XBn InAsSb DETECTORS

Production wafers of n-type InAs$_{0.91}$Sb$_{0.09}$ XBn structures are grown nearly latticed matched to 3$''$

(c.7.6-cm) GaSb substrates, in a Veeco Gen 200 MBE machine. The principal layers in the XBn structures are a thick (3–4 μm) n-type InAs$_{0.91}$Sb$_{0.09}$ photon absorbing AL, a thin n-type AlSb$_{0.91}$As$_{0.09}$ BL, and a thin n-type InAs$_{0.91}$Sb$_{0.09}$ CL. For the HOT Pelican D FPA, the grown wafers are processed into 640 $\times$ 512 pixel arrays, with a 15-μm pitch. In all cases, mesas are etched to a depth greater than the thickness of the CL, and a common contact is made to the AL outside the active device area. The arrays are flip-chip bonded with indium bumps to the digital HOT Pelican-D ROICs. After glue under-fill, the substrate is thinned and an antireflection coating is applied.

Figure 1 shows a plot of the logarithm of the dark current at an operating bias of -0.1 V versus the inverse temperature for two nominally identical nBn test devices where the CL and AL are both made from n-type InAs$_{0.91}$Sb$_{0.09}$. The devices only differ in the polarity of the BL doping. The red curve is for a p-type BL while the blue is for n-type. In each case, the band profiles are shown schematically as insets next to the curves. For the p-type BL, a p–n junction is formed with the n-type AL, resulting in a depletion region that extends some distance into the AL, shown shaded in the upper inset. The corresponding curve in the plot exhibits two straight line regions, where the slope reduces by a factor of $\sim$2 at low temperatures. The upper region can be fitted to a dependence of the form $J \propto T^3 \mathrm{e}^{-\Delta E/kT}$, in which ΔE is close to the bandgap of the AL (when extrapolated to zero temperature) and is typical of diffusion current. The lower region is typical of G–R behavior, and varies as $J \propto T^{3/2} \mathrm{e}^{-\Delta E/2kT}$ (see Ref. 4). The blue curve shows how the G–R current is suppressed by doping the BL n-type. In this case, there is no depletion of the AL, and diffusion behavior with a single slope is maintained over the whole current range. The enlarged points are for a temperature of 150 K. At this temperature, the device with a p-type BL has a dark current which is about 100 times larger than that for the n-type BL. A typical photocurrent at F/3 and 70% average quantum efficiency (QE) is 6×10^{-6} A/cm^2, corresponding to a background-limited performance (BLIP) temperature (dark current = photocurrent) for the device with the n-type BL of about 175 K. The BLIP temperature is reduced by $\sim$35 K when the BL is doped p-type. A properly designed nBn detector is thus an entirely unipolar device in which all layers are doped n-type.

The current density at 150 K for the n-type BL in Fig. 1 corresponds to a dark current of approximately 50 fA in a 15-μm FPA pixel. Figure 2a shows a histogram of the dark current distribution over all the pixels of a 640 $\times$ 512/15-μm format XBn FPA at 150 K. In this case, the mean dark current is 200 fA which can be attributed to a slightly larger cut-off wavelength for the FPA. The full width at half maximum of the distribution is 15% which is quite narrow, as required for good FPA stability against small temperature fluctuations.
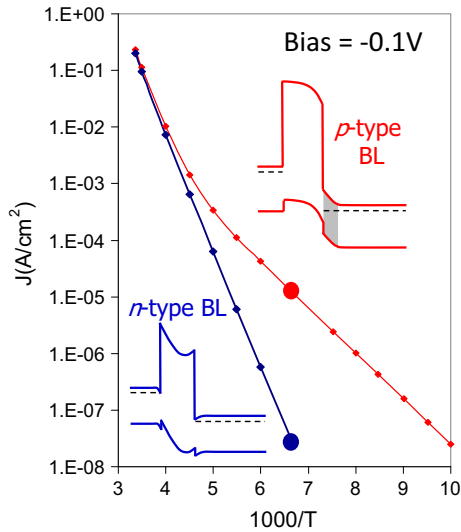
Fig. 1. Logarithm of the dark current at an operating bias of -0.1 V versus inverse temperature for two nominally identical InAs$_{0.91}$Sb$_{0.09}$ nBn test devices with opposite barrier doping polarities. The red curve is for a p-type BL (red inset with shaded depletion of AL) and the blue curve is for an n-type BL (blue inset with no depletion of AL). The enlarged points indicate a temperature of 150 K (Color figure online).

Fig. 2. (a) Typical dark current distribution for a 640 × 512 InAs$_{0.91}$Sb$_{0.09}$ XBn FPA at 150 K and (b) mean spectral response compared with an OTM response calculation.

Figure 2b shows the spectral response measured at 150 K and averaged over all FPA pixels for the same format as in Fig. 2a. This is compared with the simulated response, based on the optical transfer matrix (OTM) method described in Ref. 7. It can be seen that the cut-off wavelength (at 50% of the initial rise) is ~4.2 μm and that the QE is above 70% for wavelengths shorter than 4.15 μm. This result also justifies the conservative value of 70% used above to estimate the BLIP temperature.

Figure 3a shows both the mean NETD of all pixels at F/3.2, and the pixel operability, as a function of temperature for a 15-μm pitch Pelican-D XBn FPA. The operability is determined after performing a standard 2 point non-uniformity correction (2PC). The NETD and operability only begin to change above 170 K, consistent with the BLIP temperature of 175 K estimated above. In Fig. 3b, the pixel operability at 150 K is shown for 50 FPAs taken from a single batch of our XBn production line. It can be seen that nearly all have values greater than 99.8%, and that more than half are above 99.9%. This result highlights the robustness of the FPA fabrication process. The process yield including crystal growth is quite similar to that for our standard planar InSb production line.

The InAs$_{0.91}$Sb$_{0.09}$ material in an XBn detector has a large absorption coefficient, allowing a high QE to be achieved using a relatively thin AL. The thin AL results in a low pixel crosstalk with only 7% of incident power reaching the nearest-neighbor pixel compared with 64% in the central pixel.[8] The modulation transfer function (MTF) at 150 K for a HOT Pelican D XBn detector is plotted in Fig. 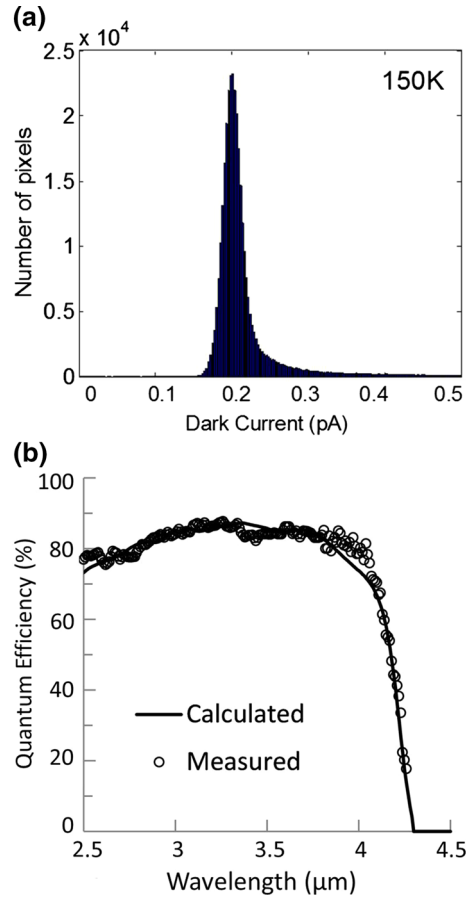4a. The crosstalk and point spread function (PSF) were measured as described in Ref. 8 and the MTF was then obtained from a Fourier transform of the PSF. The MTF at the Nyquist frequency, indicated by a red vertical dashed line, is 49% which is reasonably close to the ideal value of 63% shown in the dashed curve. Figure 4b shows the residual non-uniformity (RNU) as a percentage of the dynamic range (DR) for a Pelican D FPA after a 2PC was performed at well fill (WF) values of 13% and 80%. It can be seen that the maximum RNU/DR is less than 0.015%, corresponding to a very low level of spatial non-uniformity. There are several examples of images in the literature registered with a HOT Pelican D XBn detector. Reference 8 shows a high image quality at F/3.2 that only begins to degrade noticeably above ~190 K.

The larger format digital XBn HOT Hercules detector has 1.3 megapixels with a 15-μm pitch.[9] Its performance parameters are very similar to those presented above for HOT Pelican D and are discussed in detail in Ref. 9. In that case, a maximum RNU/DR of ~0.015% was reported, using WF values for the 2PC similar to those used above for Pelican D in Fig. 4. Figure 5 shows an example of a high-
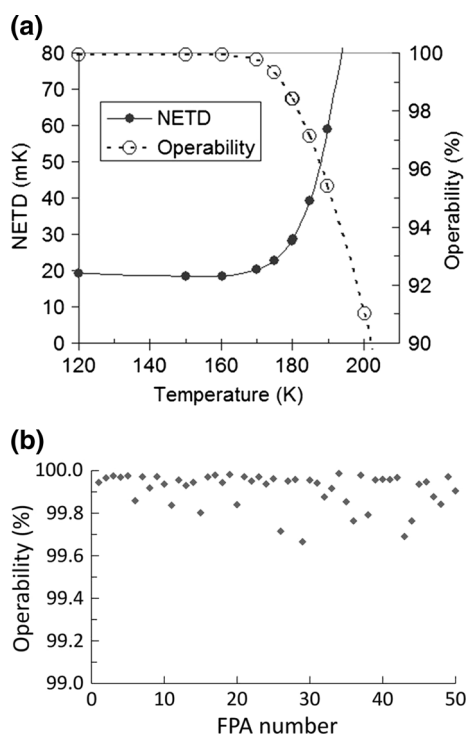
Fig. 3. (a) Temperature dependence of NETD and pixel operability for a 640 × 512 XBn FPA, measured with an aperture of F/3.2 in front of a black body at a temperature of 50°C and (b) pixel operability at 150 K, in 50 FPAs taken from a single batch of our XBn production line.
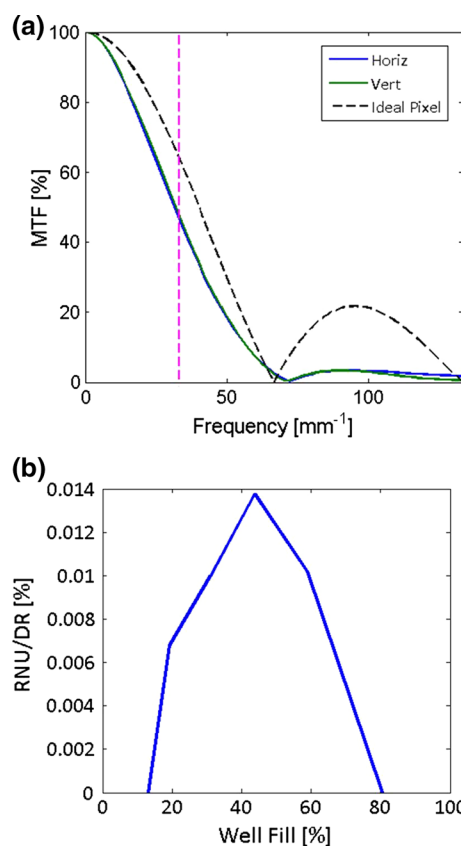

Fig. 4. (a) Detector MTF (after deconvolution of the MTF of the F/3.7 optics used in the measurement) for a wavelength window of 3.17-3.75 μm on an XBn Pelican D FPA at 150 K. (b) RNU plot for a similar detector.

definition image registered with a HOT Hercules detector at 150 K.

Table I compares some of the key properties of integrated detector cooler assemblies (IDCAs) based on standard InSb diode and InAs$_{0.91}$Sb$_{0.09}$ XBn device architectures. It can be seen that there are clear size, weight and power (SWaP) advantages for XBn IDCAs. For the same 640 × 512/15-μm FPA format, the IDCA weight is reduced by nearly 40%, the power by 50% and the mean time to failure (MTTF) is increased by more than 100%. Although the 4.2-μm cut-off wavelength of the InAs$_{0.91}$Sb$_{0.09}$ XBn detector is shorter than that of InSb, it is shown in Ref. 8 that, for many scenarios, the detection and identification ranges for both types of detector are similar, even for a scene temperature as low as −20°C. For higher scene temperatures, the XBn detector even has a slight advantage. The reason for this is that its cut-off wavelength is well matched to the more transparent upper atmospheric window of the MWIR wavelength range. The detector is therefore more immune to atmospheric noise.

Overall, the high operability, low SWaP and good reliability of InAs$_{0.91}$Sb$_{0.09}$ XBn IDCAs make them particularly attractive for 24/7 surveillance, small payloads, and long-range detection applications, in addition to the many traditional applications of MWIR detectors.

Fig. 5. Image registered with a 1280 × 1024 HOT Hercules XBn FPA at F/3 and 150 K.

XBp TYPE II SUPERLATTICE DETECTORS

A semiconductor superlattice structure based on alternating layers of InAs and GaSb, also known as a type II superlattice, exhibits rather unique

Table I. Comparison of some of the key properties of Pelican-D and Hercules IDCAs based on standard InSb diode and InAs$_{0.91}$Sb$_{0.09}$ XBn device architectures

Parameter	Standard InSb	XBn	Standard InSb	XBn
Format (μm)	640 $\times$ 512/15		1280 $\times$ 1024/15	
Cooler type	K561	K562S	K548	K508N
Weight (g)	450	280	820	730
FPA operating temperature (K)	77	150	77	150
Frame rate (Hz)	50	50	60	100
Typical total power requirement (23°C) (W)	3.8	2.3	10	3
Typical cool down time (min)	7	4	8	<10[a]
Reliability (MTTF) (h)[b]	5,000	>10,000	12,000	>26,000

[a]Optimized for 24/7 applications. [b]Under standard conditions.

properties, including a zero bandgap at a critical value of the layer thicknesses. In this respect, the T2SL bears a close relationship to the alloy, Hg$_x$Cd$_{1-x}$Te (MCT), where the bandgap vanishes at a critical value of the composition parameter, x (see Fig. 6a). As shown schematically in Fig. 6b, the superlattice bandgap can be tuned by a suitable choice of the InAs and GaSb layer thicknesses to cover the whole of the MWIR and LWIR wavelength ranges. T2SL devices are grown at SCD by MBE on commercial 3″ (c.7.6-cm) GaSb substrates. A Veeco GenIII MBE system was used during the device development stage, and a Veeco Gen 200 system is now in the process of production qualification, since it can accommodate 7 $\times$ 3″ (c.18 $\times$ 7.6 cm) substrates in a single growth run. Further growth details may be found in Ref. 10.

In order to achieve low dark currents, an XBp device architecture is used so that the dark current is diffusion-limited in a similar way to that for the MWIR XBn devices described in the previous section.[4] In this case, the AL and BL are p-type in order to exploit the larger minority carrier mobility of the conduction band, and the barrier is now in the valence band. The barrier material is an InAs/AlSb type II superlattice structure. To ensure correct band alignment, we have developed a k · p model which can also predict the absorption spectrum and cut-off wavelength of each T2SL, from a knowledge of the thicknesses of the InAs and GaSb or AlSb in each superlattice period. We have also developed an OTM calculation which predicts the full spectral response of the back illuminated detector, based essentially on the calculated absorption spectrum and the AL stack thickness. Further details are given in Ref. 11.

In addition to the development of design tools for a T2SL device with an XBp architecture, we have also developed a custom ROIC and a robust passivation process that prevents device degradation after ROIC hybridization, glue under-fill and substrate thinning.[12] The ROIC has been designed so that the complete detector closely follows the interfaces of SCD's MWIR Pelican-D detector family.
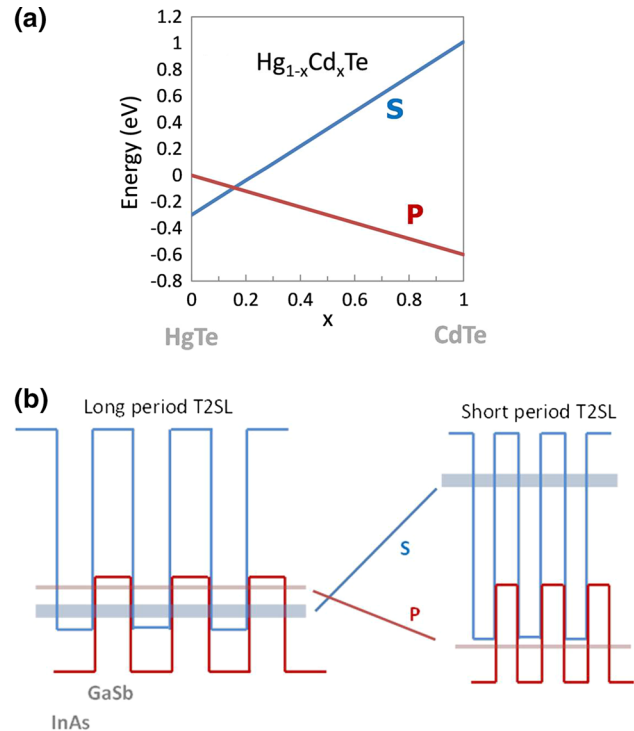
Fig. 6. Depiction of the existence of a zero bandgap state which occurs when the bands with s- and p-like orbital symmetry cross at a critical value of (a) the composition parameter, x, in Hg$_{1-x}$Cd$_x$Te and (b) the InAs and GaSb layer thicknesses in a type II superlattice.

Figure 7 compares the logarithm of the dark current versus the inverse temperature for a pBp test structure and for a n-on-p test photodiode made with nominally the same T2SL AL layer material (cut-off wavelength = 10 μm). The barrier in the pBp structure is p-type. The curve for this device exhibits a single straight line characteristic of diffusion limited behavior over the whole temperature range, while the photodiode has a smaller slope at low temperatures characteristic of G–R behavior. The plots are very similar in character to those shown in Fig. 1 for XBn devices and, in each case, a BL with the same doping as the AL is able to
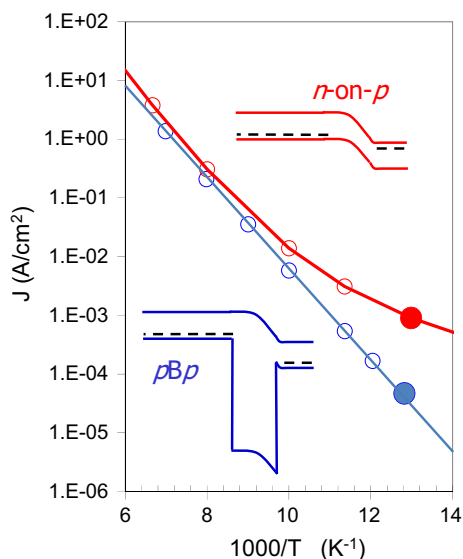
Fig. 7. Logarithm of the dark current versus inverse temperature in a pBp test device (blue curve, bias = 0.6 V) and n–p test diode (red curve, bias = 0.1 V), each with an InAs/GaSb active layer bandgap wavelength of $\lambda_G \sim 10$ μm and a mesa area of 100×100 μm^2. The enlarged points indicate a temperature of 77 K (Color figure online).

suppress the G–R contribution. In the present case, the dark current at 77 K for the barrier device is 20 times smaller than for the photodiode (large circles in Fig. 7).

Figure 8 shows dark current densities for FPAs with cut-off wavelengths between 8.7 μm and 10.3 μm on a Rule 07 plot,[13] together with corresponding results from test devices spanning a similar wavelength range. In each case, the cut-off wavelength (in μm) is given in the legend, as measured by photoluminescence spectroscopy at $\sim$10 K, and, for the FPAs, the number of FPAs measured is also stated. The standard deviation of the FPA dark current is plotted as positive and negative error bars, and is generally quite small. It can be seen that the distributions of FPA and test device results fall in the same range which is slightly more than one order of magnitude above the solid blue Rule-07 line.

Figure 9 compares the spectral response of a Pelican-D LW FPA measured at 77 K with the simulated spectrum based on the k · p and OTM calculations described above. The measurement was performed using a Bruker Equinox FTIR spectrometer and is quite noisy due to a weak globar source and to some atmospheric absorption along the measurement path. Nevertheless, it can be seen that very good agreement is obtained by the simulation, for a T2SL with a cut-off wavelength of 9.46 μm. The fitted inhomogeneous broadening at the band edge was 10 meV, which agrees very well with the fluctuations in the band edge energies calculated from the k · p model caused by single monolayer interface steps.[12] The maximum QE in the measured spectrum is 60%. The Pelican-D LW FPA has an AL thickness of 4.5 μm, and the current
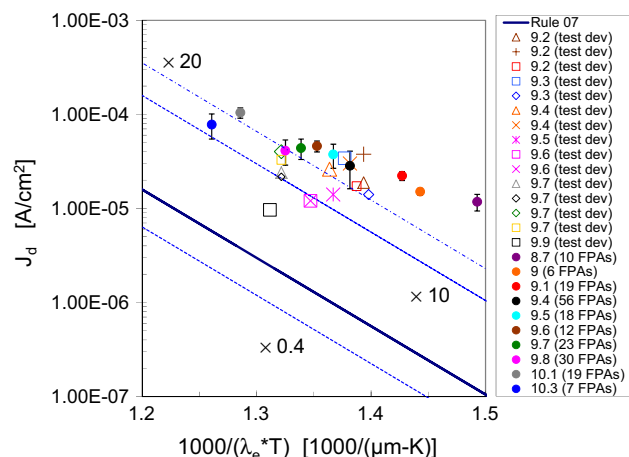

Fig. 8. Comparison of T2SL dark current with MCT Rule 07 (solid blue line) for test devices and FPAs with device cut-off wavelengths as indicted in the legend (Color figure online).
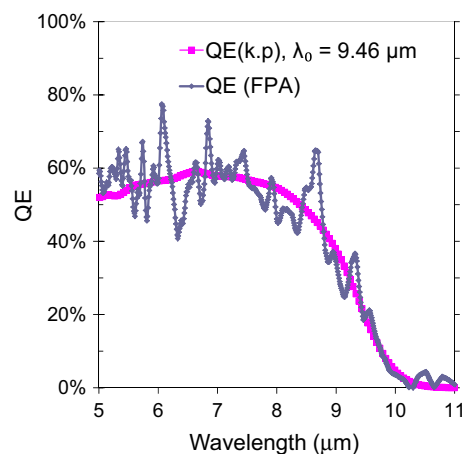

Fig. 9. Quantum efficiency at 77 K for a one-pass detector with AL = 4.5 μm as a function of wavelength, comparing measured spectrum (blue) and simulation based on k · p theory (purple) (Color figure online).

version is a one-pass device in which the incident radiation only passes once through the AL. A two-pass device is currently under development.

At 65% well fill of its 6Me$^-$ capacitor and a frame rate of 240 Hz, Pelican-D LW offers an NETD of 36 mK when configured with F/2.7 optics. By averaging 8 frames at a time, the detector operates at an effective frame rate of 30 Hz. The NETD distribution measured under these conditions for the Pelican-D LW FPA is shown in Fig. 10. The distribution is narrow and symmetric with no pronounced tailing. The peak value is 13 mK which is a reduction of $\sqrt{8}$ relative to the single frame value. This is as expected for pure shot noise, and shows that any noise introduced by the averaging procedure is negligible.

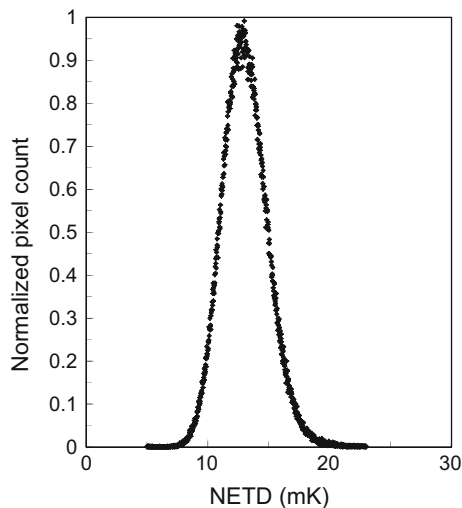The RNU of the Pelican D LW FPA has been measured after performing a 2PC. The magenta line

Fig. 10. NETD distribution of the Pelican-D LW T2SL FPA at 77 K, F/2.7 and a frame rate of 30 Hz.

Fig. 12. Distribution of NETD (blue) and pixel operability (red) values for 75 Pelican-D LW FPAs from the new SCD production line (Color figure online).
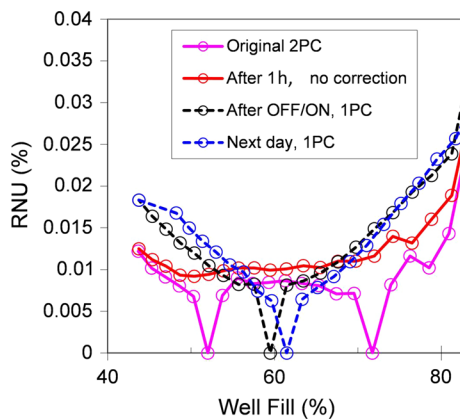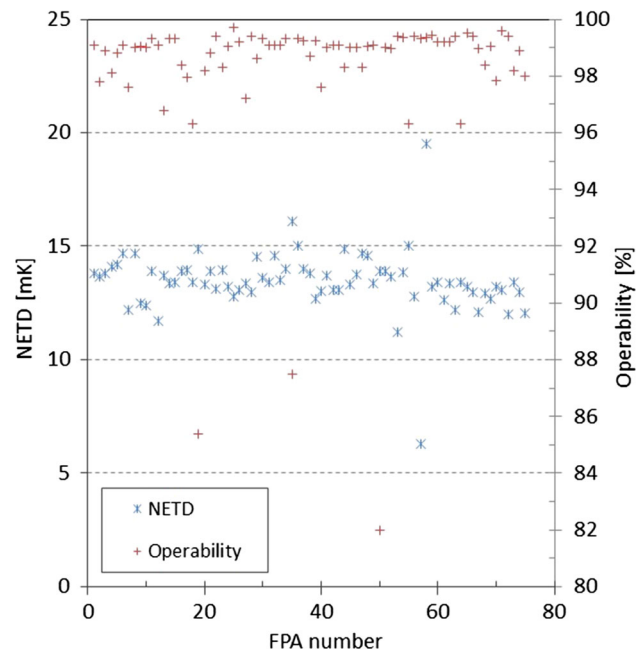

Fig. 11. RNU of Pelican-D LW IDCA at 77 K after performing a 2PC at 52% and 72% well fill (magenta); 1 h later with no correction (red); after turning off and on with a 1PC (black dash); after turning on the next day with a 1PC (blue dash) (Color figure online).

Fig. 13. Image registered with a demonstration camera containing the 15-μm pitch, 640 × 512 Pelican-D LW FPA, operating with improvised (non-optimum) F/2.7 optics at 77 K.

in Fig. 11 shows a plot of RNU versus WF for an IDCA measured using different black body temperatures and a constant integration time. The 2PC was performed at WF values of 52% and 72%, respectively. The RNU remains below 0.02% of the DR for WF values in the range 40–80%. Moreover, the image is very stable for many hours without any further corrections, as shown by the red line, which was registered 1 h after the 2PC was performed. The dashed lines show RNU curves after switching the detector off and then immediately back on (black), or back on the next day (blue), and performing only a one-point offset correction (1PC). In all cases, the RNU curves remain within ∼0.01% of the original calibration curve.

Figure 12 shows the distributions of NETD and operability values for the first 75 Pelican-D LW FPAs from our new production line. Only 2 FPAs exhibit an NETD of more than 15 mK, and more

than 65% of the FPAs have an operability above 99%. Several FPAs have operability values above 99.5% and a program is underway to increase the proportion of FPAs in this operability range. The operability is defined according to SCD's production line criteria. These criteria include stringent limits on pixel signal, responsivity, noise, NETD, and uniformity of the corrected image.

In Fig. 13, we show an image registered with a demonstration camera containing a Pelican-D LW FPA operating at 77 K. A table with full details of the current performance specification may be found in Ref. 12.

CONCLUSIONS

Over the past decade, SCD has developed high-end MWIR and LWIR detectors based on III–V materials, which exhibit very low dark currents and high quantum efficiencies. Unique challenges for such detectors are the suppression of the G–R contribution to the dark current and the development of a reliable and robust surface passivation process. The former has been achieved by using a patented XBn/XBp device architecture, yielding MWIR dark currents in agreement with MCT Rule 07 and LWIR dark currents which are only 10–20 times greater. Corresponding operating temperatures are 150 K for an XBn detector with a 4.2-μm cut-off, and 77 K for an XBp detector with a 9.3-μm cut-off. In each case, the operating photocurrent to dark current ratio is greater than 10, and the implementation of a robust passivation process has led to very stable operation, with RNU/DR values of $\sim$0.02%, even after several shut-down cycles.

Two MWIR FPA formats with a 15-μm pitch are currently in production, HOT Pelican D with 0.33 megapixels and HOT Hercules with 1.3 megapixels. A 3-megapixel/10-μm version is currently completing development. The digital MWIR IDCAs offer large SWaP advantages, including much lower power and a much longer MTTF compared with standard InSb IDCAs. Together with their ability to operate in one of the most transparent atmospheric windows, these features make the HOT XBn detectors particularly attractive for applications such as 24/7 surveillance, small payloads, handheld devices, and long-range observation.

The Pelican D LW detector has been designed to follow closely the interfaces of SCD's MWIR Pelican-D family, enabling fast system integration. The current version has a QE of $\sim$50%, an NETD of 13 mK at F/2.7 and 30 Hz, and an operability above 99%. The highly reproducible results from our new LWIR detector production line show that T2SL materials can now be considered to be a realistic alternative to MCT for small-pitch, high-performance single and dual-color FPA detectors.

REFERENCES

1. D.A. Reago, (2008), http://spie.org/x20227.xml.
2. P.C. Klipstein, US Patent 7,795,640 (2003).
3. P.C. Klipstein, US Patent 8,004,012 (2006).
4. P.C. Klipstein, O. Klin, S. Grossman, N. Snapi, I. Lukomsky, M. Yassen, D. Aronov, E. Berkowicz, A. Glozman, O. Magen, I. Shtrichman, R. Fraenkel, and E. Weiss, *Proc. SPIE* 8268, 8268-0U (2012).
5. P.C. Klipstein, *Proc. SPIE* 6940, 6940-2U (2008).
6. L. Shkedy, M. Brumer, P.C. Klipstein, M. Nitzani, E. Avnon, Y. Kodriano, I. Lukomsky, and I. Shtrichman, *Proc. SPIE* 9819, 9819-1D (2016).
7. P.C. Klipstein, O. Klin, S. Grossman, N. Snapi, B. Yaakobovitz, M. Brumer, I. Lukomsky, D. Aronov, M. Yassen, B. Yofis, A. Glozman, T. Fishman, E. Berkowicz, O. Magen, and I. Shtrichman, E Weiss (2010). *Proc. SPIE* 7608, 7608-1V (2010).
8. P.C. Klipstein, Y. Gross, D. Aronov, M. Ben Ezra, E. Berkowicz, Y. Cohen, R. Fraenkel, A. Glozman, S. Grossman, O. Klin, I. Lukomsky, T. Markowitz, L. Shkedy, I. Shtrichman, N. Snapi, A. Tuito, M. Yassen, and E. Weiss, *Proc. SPIE* 8704, 8704-1S (2013).
9. Y. Karni, E. Avnon, M. Ben Ezra, E. Berkowicz, O. Cohen, Y. Cohen, R. Dobromislin, I. Hirsh, O. Klin, P.C. Klipstein, I. Lukomsky, M. Nitzani, I. Pivnik, O. Rozenberg, I. Shtrichman, M. Singer, S. Sulimani, A. Tuito, and E. Weiss, *Proc. SPIE* 9070, 9070-1F (2014).
10. O. Klin, N. Snapi, Y. Cohen, and E. Weiss, *J. Cryst. Growth* 425, 54 (2015).
11. Y. Livneh, P.C. Klipstein, O. Klin, N. Snapi, S. Grossman, A. Glozman, and E. Weiss, *Phys. Rev. B* 86, 235311 (2012); Erratum, *Phys. Rev. B* 90, 039903 (2014).
12. P.C. Klipstein, E. Avnon, D. Azulai, Y. Benny, R. Fraenkel, A. Glozman, E. Hojman, O. Klin, L. Krasovitsky, L. Langof, I. Lukomsky, M. Nitzani, I. Shtrichman, N. Rappaport, N. Snapi, E. Weiss, and A. Tuito, *Proc. SPIE* 9819, 9819-0T (2016).
13. W.E. Tennant, *J. Electron. Mater.* 39, 1030 (2010).